Japanese Journal of Applied Physics **50** (2011) 06GL05 **REGULAR PAPER**
DOI: 10.1143/JJAP.50.06GL05

Fabrication of Microfluidic Platform with Optimized Fluidic Network toward On-Chip Parallel Systematic Evolution of Ligands by Exponential Enrichment Process

Tae Kyung Kim, Sang Wook Lee[1], Ji-Young Ahn[2], Thomas Laurell[1], So Youn Kim[2], and Ok Chan Jeong*

Department of Biomedical Engineering, Inje University, Gimhae, Gyungnam 621-749, Korea
[1]*Department of Electrical Measurements, Lund University, Lund 22184, Sweden*
[2]*Department of Biomedical Engineering, Dongguk University, Seoul 100-715, Korea*

Received November 29, 2010; accepted March 2, 2011; published online June 20, 2011

This paper presents the design and fabrication of a microplatform with the optimal fluidic network for an on-chip parallel "systematic evolution of ligands by exponential enrichment" (SELEX) process. The effectiveness of the optimized fluidic network for on-chip five-plex aptamer screening was verified by measuring the airflow rate at the elution ports and visualizing the specific elution during the SELEX process. The proposed device with an optimally designed hydraulic resistance-balanced channel network could be feasible and utilized as a multiplex selection module for a parallel SELEX process. © 2011 The Japan Society of Applied Physics

1. Introduction

Recently, interest in the development of microfluidic "systematic evolution of ligands by exponential enrichment" (SELEX) systems has been growing.[1)] Because of microfluidics, microfabricated systems for controlling fluid at microscale levels have significant advantages in terms of reaction speed, high-throughput, yield, selectivity, and controllability.[2)]

One of the more interesting microfluidic devices in microelectromechanical systems (MEMS) and total analysis systems (TAS) is microfluidic platforms for an aptamer SELEX process.[3)] Aptamers are smaller and more stable compared to antibodies. Because they also have high affinity and specificity, they have high potential for diagnostic,[4)] therapeutic,[5)] and bioanalytical applications.[6)] In one study,[3)] the developed device was comprised of a microheater and five sol–gel chambers as serial simple microchannel-crossing chambers for the SELEX process. However, there was a major drawback of this previous work. The parallel operation of the SELEX process was very difficult because all chambers were connected and there was a single elution port. Compared with the aptamer selection technique against a single target molecule, the multiplex SELEX process enables rapid isolation of large numbers of distinct aptamers among multiple targets. Thus, it could provide an effective method for the rapid SELEX process. In order to resolve this weak point and demonstrate a multiplex SELEX process, our group fabricated a microfluidic platform for a parallel five-plex SELEX process, and demonstrated its successful parallel operation.[7)] The proposed device was integrated with an electrical heater, a pneumatically-driven poly(dimethylsiloxane) (PDMS) diaphragm valve,[8)] and a pressure-driven microfluidic channel. The rubber-seal pneumatically driven PDMS valve[9–14)] was a key component that was designed to prevent cross-contamination of the reaction chamber caused by possible leakage of fluid containing specific aptamers bound to the target protein. However, there was one disadvantage in the usage of the microplatform for the SELEX process. During the elution process of the target-bound aptamers, the eluted volumes at each elution port were different. Thus, an additional process such as repeated manual switching actions of the tubes connecting with the elution ports was necessary to obtain the proper elution volumes at the five different ports, and the operation time for the elution process increased. Equal eluted volumes at each elution port are essential in a fully automated and quantitative microplatform for the SELEX process.

This paper presents a structural design for a fluidic network that ensures an efficient elution process based on the analog between electric and hydraulic systems. An analytical model using basic circuit theory was confirmed by computational analysis. A fully integrated microfluidic platform with an optimized fluid network for the on-chip aptamer SELEX process was fabricated. The fabricated microfluidic platform were tested to verify the structural design of the fluidic network.

2. Parallel SELEX on Chip

2.1 Device structure

Figure 1 shows the microfluidic platform and its three-dimensional schematic view. The microfluidic platform for the SELEX process on a chip was integrated with functional parts, such as microresistive heaters on glass substrate, a microfluidic network with sol–gel chambers, and pneumatic valves. The microfluidic platform can provide fluidic operations for a multiplex SELEX process, such as fluidic injection and incubation for the binding process of RNA aptamers and target proteins, washing to remove unbound RNA, and elution of bound DNA aptamers. During the parallel elution process in the fluidic operation, the rubber-seal pneumatically driven PDMS valves were used to isolate the parallel chambers to prevent unwanted cross-contamination and mixing of the individual fluids containing specific bound DNA aptamers.

2.2 Fabrication and integration

Figure 2 shows the assembly sequence of the microfluidic platform for the SELEX process. To prepare the liquid PDMS (Dow Corning Sylgard 184), a base polymer was mixed with a curing reagent. After the removal of trapped air bubbles inside the mixture of liquid PDMS, the prepared liquid PDMS was poured onto an SU-8 mold (MicroChem SU-8 2075) for various ports, the valve chamber, and the fluid network layer; spin-coated; and then cured at 75 °C for 2 h. There were three step-bonding processes for the

*E-mail address: memsoku@inje.ac.kr

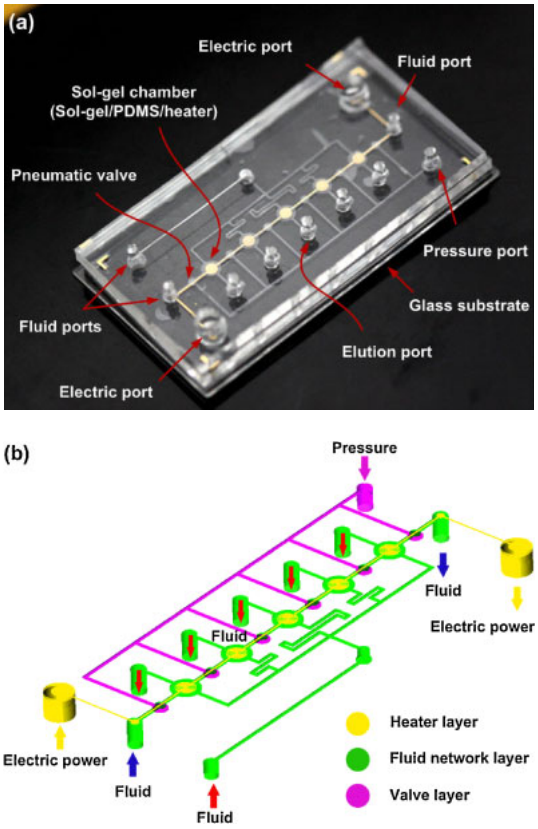

Fig. 1. (Color online) Parallel SELEX on a chip with the hydraulic resistance-balanced channel network. It consists of the three major components for the parallel selection of five target aptamers: a sol–gel chamber, an electrical heater, and a pneumatic valve. (a) Fabricated chip; (b) schematic view showing the three-dimensional layout of the SELEX chip.

SELEX chip. First, both surfaces of the valve chamber layer and the fluidic network layer were modified with oxygen plasma after peeling off the cured valve chamber layer from the SU-8 mold. The two plasma-treated layers were aligned and lowered onto the fluidic layer for the bonding process. The bonded structure was peeled from the SU-8 mold for the fluidic network. Second, the bonded PDMS structure was bonded to the various port layers after plasma treatment. After the bonding processes, the essential through-holes for electric power ports, the fluid ports for liquid sample injection, and the pneumatic port were punched out. The height of the SU-8 molds for the sol–gel chamber, valve chamber, and elution channel were 59, 37, and 114 μm, respectively. The thickness of the valve diaphragm in the fluidic network layer was 45 μm. The diameter of the reaction chamber and fluid channel were 1 mm and 100 μm, respectively. For the microheater, a Cr/Au layer (100/1000 Å) was deposited on a glass substrate and patterned. The line width of the heater pattern was 50 μm, and the total resistance of the serially connected five microheaters was 287 Ω at room temperature. Next, a 100-μm PDMS layer was coated on the heater pattern and cured for heater protection from the joule heating and the absorption layer for the sol–gel droplets. Finally, the bonding process of the prepared bonded PDMS structure and the microheater substrate after spotting sol–gel droplets on the microheater pattern was performed.

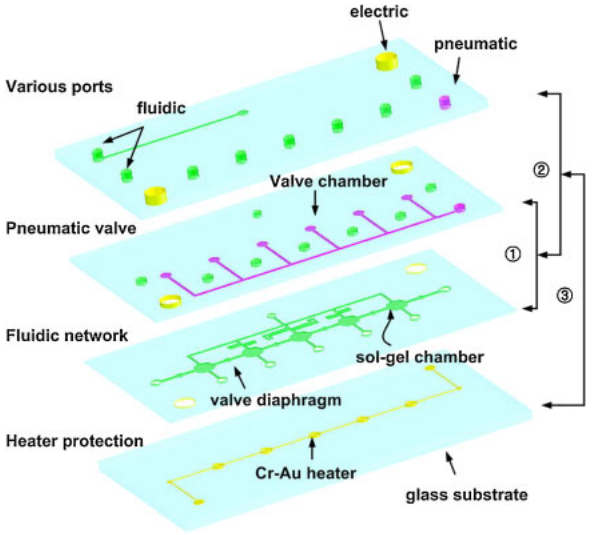

Fig. 2. (Color online) Assembly sequence of SELEX on a chip. The four PDMS layers for various ports, valve chamber, fluidic network, and heater protection/sol–gel dropping substrate are fabricated through a soft lithography method. The prepared PDMS layers are aligned carefully and then bonded sequentially with an atmosphere pressure plasma machine. The surface modification time is a few seconds.

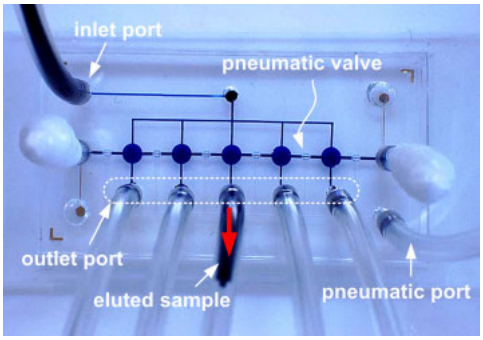

Fig. 3. (Color online) Visualization of the elution process using a microfluidic platform with a simple channel network.[7] After valve action, the injected fluid from the inlet port is first eluted at the central elution port because of the complex and unbalanced hydraulic resistance of the microchannel network. Thus, the flow rate at the central elution port is much larger than at other ports.

2.3 Design issue in fluid network

As previously stated, there is one drawback to the usage of microplatforms for the parallel SELEX process.[7] As shown in Fig. 3, the traveling times in the fluidic network from the elution inlet to each outlet port differ during the elution process. This is caused by the fluidic resistance difference between each elution port in the fluid network. Thus, the elution volume at the central elution port is much larger than at other ports. To overcome this problem, a structural design of the fluid network for the elution process is required for the effective SELEX process.

2.3.1 Electrical model

Figure 4 shows an electrical model of the microfluidic channel network after operation of the micropneumatic valve. To understand and resolve the phenomenon shown in Fig. 3, the microfluidic network was modeled using analogs between electric and hydraulic systems.[15–17] Assuming that

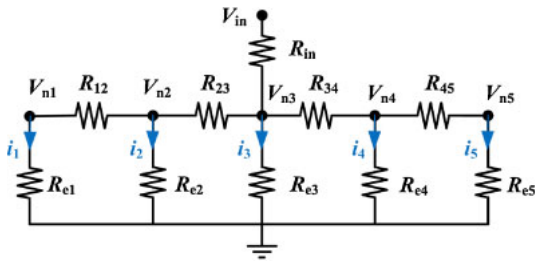

Fig. 4. (Color online) Electric model of the fluidic network in the microchip after the valve operation. The hydraulic resistance, R (Pa sm^{-3}) depended on the physical shape and the length of the microchannel.[15,19,20] $R_{in} = 1.55 \times 10^{11}$ Pa sm^{-3}, $R_{12} = R_{23} = R_{34} = R_{45} = 3.45 \times 10^{11}$ Pa sm^{-3}, and $R_{e1} = R_{e2} = R_{e3} = R_{e4} = R_{e5} = 1.52 \times 10^{11}$ Pa sm^{-3}.

there was no structural deformation of the PDMS channel, the fluidic network could be modeled as a simple fluidic resistance network without any capacitance or inertial effects.[18] To minimize and prevent a time-delay effect in the microchannel network, silicon hybrid PDMS (mixed with excess curing agent) was used to fabricate the microchannel network. In Fig. 4, when 1 V of voltage was applied, the node voltages V_{n1}, V_{n2}, and V_{n3} were 0.289, 0.073, and 0.002 V, respectively. Thus, because node voltages V_{n1}, V_{n2}, and V_{n3} were different, so was the current passing the resistances at the elution ports. Therefore, the flow rate of the elution volumes at each port was different.

In order to obtain the same elution volume or flow rate, the electrical resistances between the elution inlet port and the outlet ports were adjusted by properly increasing the length of the microfluidic channel. Moreover, the channel width increased two-fold for the flow rate increment of the eluted samples. Unlike the microfluidic channel network with the same resistances shown in Fig. 3, in the newly fabricated microfluidic channel network, R_{e2} ($= R_{e4}$) and R_{e3} increased by 3.27 and 6.82 times, respectively. R_{e1} ($= R_{e5}$) remained the same. Thus, the current passing all resistances to the elution ports was the same.

2.3.2 Simulation

Figure 5 shows finite element model (FEM) analysis results (COMSOL FEMLAB) for the velocity field of the fluid and a three-dimensional view of its highlights in the microchannel network. Before the operation of valve (a), the applied pressure at the inlet port was gradually reduced along the complex microchannel network. The central port was larger than the other ports; therefore, the velocity field of the working fluid at the central elution port was slightly larger than others. However, once the microchannel between two chambers was closed by operation of the microvalve, the hydraulic resistance in the microchannel network was changed by the simple combination of parallel resistances, as shown in Fig. 4. Thus, the velocity field at the central elution port was much larger than the others because of the traveling path of the pressure-driven fluid flow (b). As previously discussed, the length of the microchannel increased due to the adjustment of the hydraulic resistance after the valve operation (c). Even though the microvalve was operated, the velocity field at all ports was the same as designed. Both the

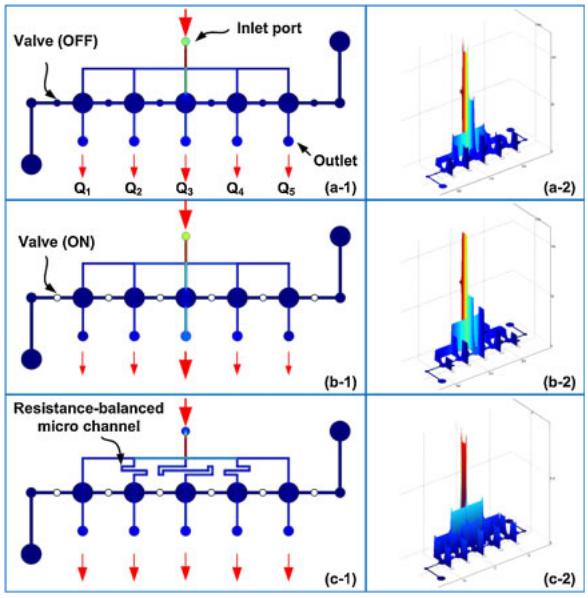

Fig. 5. (Color online) FEM analysis results (left-1) for the velocity field; (right-2) three-dimensional view of the flow. A general laminar flow model in the MEMS module was used to analyze the fluid network. The working fluid was water, and the applied pressure at the inlet port was 100 Pa. (a) In a simple network before the operation of the microvalve; (b) in a simple network after operation of the microvalve; (c) in the fluid network with a resistance-balanced channel structure.

electrical model and computational analysis confirmed the effectiveness of the design method for a successful elution process using a pure resistance-balanced channel network.

3. Experiment

Although the fabricated microfluidic platform had many possible applications, including electrical heating and pneumatic valve operation, we focused mainly on the elution process during fluid operation in this study.

3.1 Measurement system

Various fluids and the pneumatic valve were controlled by a syringe pump and a lab-designed pneumatic control system, respectively. The external compressed air generated by an air compressor was supplied to the pneumatic valves using the switching operation of electromagnetic valves, which was controlled by Labview software. The supplied pressure was monitored with precision pressure sensors (Honeywell SDX05D4). The SELEX process was observed with a digital microscope (Hi-Rox 7700).

4. Results and Discussion

4.1 Elution process with compressed air

To verify the effectiveness of the fluidic network, the air flow rates at the outlet ports were measured with a bidirectional mass flow sensor (Sensirion ASF1430). The measurement resolution and the sampling frequency of the sensor were 0.06 sccm and 50 Hz, respectively.

Figure 6 shows the measured air flow rates at the elution ports when compressed air was supplied at the fluid port for the elution process. The magnitude, frequency, and duty ratio of the square wave input signal for applying the compressed air were 50 kPa, 0.05 Hz, and 50%, respectively. Overall, the measured signal for the flow rate of the

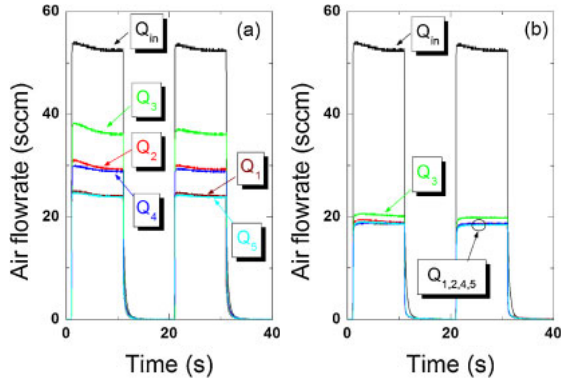

Fig. 6. (Color online) Measured airflow rates of compressed air at the elution ports. (a) Previous chip; (b) proposed chip with optimized fluid network.

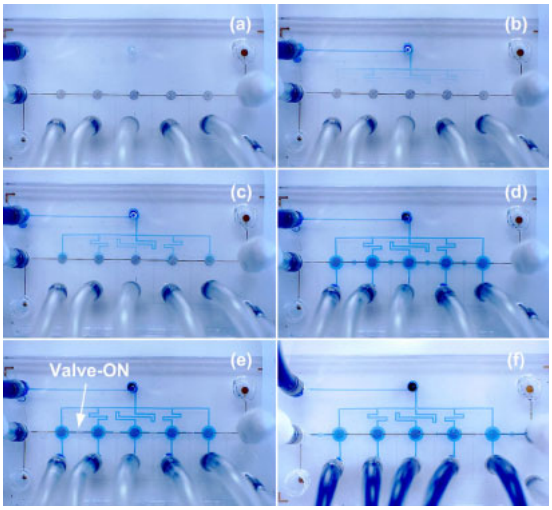

Fig. 7. (Color online) Visualization of the fluid flow in the fluidic resistance-balanced microchannel network. The currents or flow rates at all ports are almost identical to those designed. (a) Before operation; (b–f) sequential elution processes.

air stabilized from the second pulse input. As previously discussed, for our previous microfluidic platform,[7] the measured flow rate of the compressed air at the elution ports was clearly position-dependent because the flow rate of the applied air was inversely proportional to the hydraulic resistance of the microchannel. Thus, the flow rate of the air (Q_1, Q_5) was smaller than for air with a shorter fluid path (Q_2, Q_4, and Q_3). The flow rate of the air at the central port (Q_3) was largest compared to the others. In contrast, the magnitudes of the eluted flow rates of the air at every port except Q_3 were almost identical, as expected from the theoretical and computational analyses. Q_3 was larger than the others. However, the current structural design of the fluid network was acceptable for a parallel SELEX process because Q_3 was only larger by +5.88% of the magnitude of the flow rates at the other ports (Q_1, Q_2, Q_4, and Q_5).

4.2 Elution process with liquid

Figure 7 illustrates the sequential elution process of our proposed microfluidic device. Deionized water and blue ink were used for the visualization of the elution process. By taking advantage of the flexibility of PDMS, the nearly perfect rubber-seal valve[8] could be utilized for isolating the five chambers to successfully perform a parallel SELEX process with five different protein targets (e). Based on our experience,[7] there was no noticeable cross-contamination caused by leakage of fluid containing specific aptamer binding to its correspondent protein target. Unlike our previous device, the flow rate of the fluid at every port was almost identical in our experiment. As discussed in §2.3, the design for our improved microfluidic platform with well-balanced fluidic resistances effectively obtained equal volumes of elution samples at the different outlet ports. Therefore, our proposed device with an optimally designed hydraulic resistance-balanced channel network could be feasible and may be utilized as a multiplex selection module for a fully automated SELEX process.

5. Conclusions

This paper presented a fully integrated microplatform for a multiplex SELEX. The network was optimized using an analog between electrical and hydraulic systems in order to obtain equal eluted volumes for an effective elution process. The optimized structure was verified computationally and experimentally.

Acknowledgements

This work was supported by Korea Small and Medium Business Administration (No. S1072576) and Basic Science Research Program through the National Research Foundation of Korea (NRF) funded by the Ministry of Education, Science and Technology (2010-0015743).

1) G. Hybarger, J. Bynum, R. F. Williams, J. J. Valdes, and J. P. Chambers: Anal. Bioanal. Chem. **384** (2006) 191.
2) A. deMello: Nature **442** (2006) 394.
3) S. M. Park, J. Y. Ahn, M. Jo, D. K. Lee, J. T. Lis, H. G. Craighead, and S. Kim: Lab Chip **9** (2009) 1206.
4) M. Bianchini, M. Radrizzani, M. G. Brocardo, G. B. Reyes, C. Gonzalez Solveyra, and T. A. Santa-Coloma: J. Immunol. Methods **252** (2001) 191.
5) K. T. Guo, X. R. Yan, G. J. Huang, C. X. Xu, Y. S. Chai, and Z. Q. Zhang: Sheng Wu Gong Cheng Xue Bao **19** (2003) 730 [in Chinese].
6) R. Stoltenburg, C. Reinemann, and B. Strehlitz: Biomol. Eng. **24** (2007) 381.
7) S. W. Lee, J. Y. Ahn, R. Shou, E. K. Kim, T. Laurell, O. C. Jeong, and S. Y. Kim: Proc. Micro Total Analysis Systems, 2010, p. 1346.
8) O. C. Jeong and S. Konishi: Sens. Actuators A **143** (2008) 84.
9) J. C. McDonald and G. M. Whitesides: Acc. Chem. Res. **35** (2002) 491.
10) M. A. Unger, H. Chou, T. Thorsen, A. Scherer, and S. R. Quake: Science **288** (2000) 113.
11) W. H. Grover, R. H. C. Ivester, E. C. Jensen, and R. A. Mathies: Lab Chip **6** (2006) 623.
12) J. P. Urbanski, W. Thies, C. Rhodes, S. Amarasinghe, and T. Thorsen: Lab Chip **6** (2006) 96.
13) L. Kim, M. D. Vahey, H. Y. Lee, and J. Voldman: Lab Chip **6** (2006) 394.
14) J. Goulpeau, D. Trouchet, A. Ajdari, and P. Tabeling: J. Appl. Phys. **98** (2005) 044914.
15) D. Kim, N. C. Chesler, and D. J. Beebe: Lab Chip **6** (2006) 639.
16) Y. Kim, B. Kuczenski, P. R. LeDuc, and W. C. Messner: Lab Chip **9** (2009) 2603.
17) M. R. Begley, M. Utz, D. C. Leslie, H. H. Hariri, J. Landers, and H. B. Smith: Appl. Phys. Lett. **95** (2009) 203501.
18) O. C. Jeong and S. Konishi: J. Micromech. Microeng. **18** (2008) 085017.
19) K. Hattori, S. Sugiura, and T. Kanamori: Lab Chip **9** (2009) 1763.
20) M. Tencer and P. Berini: Microfluid. Nanofluid. **6** (2009) 17.